SCIENCE CHINA
Earth Sciences

•RESEARCH PAPER•

https://doi.org/10.1007/s11430-021-9956-5

Variations in terrestrial oxygen sources under climate change

Lei DING[1], Jianping HUANG[1,2*], Changyu LI[1], Dongliang HAN[1], Xiaoyue LIU[1], Haiyun LI[1], Yan BAI[1] & Jiping HUANG[3]

[1] *College of Atmospheric Sciences, Lanzhou University, Lanzhou 730000, China;*
[2] *Collaborative Innovation Center for Western Ecological Safety, Lanzhou University, Lanzhou 730000, China;*
[3] *Enlightening Bioscience Research Center, Mississauga L4X 2X7, Canada*

Received November 19, 2021; revised May 16, 2022; accepted May 30, 2022; published online August 12, 2022

Abstract The terrestrial ecosystem is an important source of atmospheric oxygen, and its changes are closely related to variations in atmospheric oxygen level. However, few studies have focused on the characteristics and driving forces behind terrestrial ecosystem oxygen sources. In this study, based on observations and net carbon flux simulations from the Sixth Coupled Model Intercomparison Project, we investigated temporal and spatial variations in terrestrial oxygen sources. As the largest source of atmospheric oxygen, the terrestrial ecosystem can produce approximately 7.10±0.38 gigatons of oxygen per year, and the tropics are the main oxygen producing regions. Notably, there are many "non-oxygen-producing lands", where the lands no longer provide oxygen to the atmosphere, located in the high latitudes and around the deserts of Central Asia. Long-term analysis reveals that anthropogenic activities and climate change are responsible for the variations in terrestrial oxygen sources owing to land-use changes and competing effects between net photosynthesis and heterotrophic respiration. By 2100, more oxygen will be produced from the low-middle latitudes, while the high latitudes will serve as a larger oxygen sink due to extreme land-use type changes and drastic increases in soil respiration. Through this study, we supplement the understanding of the modern oxygen cycle and help provide better estimates for future variations in atmospheric oxygen level.

Keywords Oxygen cycle, Terrestrial ecosystem, CMIP6, Anthropogenic forcing, Climate change

Citation: Ding L, Huang J, Li C, Han D, Liu X, Li H, Bai Y, Huang J. 2022. Variations in terrestrial oxygen sources under climate change. Science China Earth Sciences, 65, https://doi.org/10.1007/s11430-021-9956-5

1. Introduction

Oxygen (O_2) is a vital atmospheric component for all aerobic life, including human beings (Maltepe and Saugstad, 2009). As the largest source of atmospheric O_2, the terrestrial biosphere continually absorbs carbon dioxide (CO_2) and emits O_2 into the atmosphere through photosynthesis in autotrophic plants, thereby maintaining the atmospheric O_2 concentration at a safe level (Chameides and Perdue, 1997). However, since the beginning of the industrial revolution, human activities have disturbed this balance and markedly changed the modern oxygen cycle (Han et al., 2021; Huang et al., 2021). *In situ* observations have revealed that the concentration of atmospheric O_2 has declined over the past 30 years (Keeling and Manning, 2014) due to increasing fossil fuel combustion, which can consume almost 38.2 gigatons (Gt) of O_2 per year (Huang et al., 2018). However, few studies have focused on how terrestrial O_2 sources respond to anthropogenic activities and related climate change.

It is difficult to quantify changes in terrestrial O_2 sources, which involve variations in net photosynthesis and heterotrophic respiration (Rh). The O_2 produced during net photosynthesis is offset by the cost of the Rh process. Compared with preindustrial levels, the current global climate is warmer, and the atmospheric CO_2 concentration is much higher (IPCC AR5 Report, 2013), which influences both processes.

* Corresponding author (email: hjp@lzu.edu.cn)

On the one hand, net photosynthesis in plants can be improved through fertilizing effects (Smith et al., 2016), nitrogen (N) deposition (Townsend et al., 1996; Sutton et al., 2008; Whittinghill et al., 2012), and the lengthening of the plant growing season (Nemani et al., 2003; Piao et al., 2007). Additionally, precipitation increases along with enhanced evaporation over the oceans (IPCC AR5 Report, 2013), which is beneficial for tropical plant growth. On the other hand, as temperature and soil moisture are the main factors for soil respiration (Yang and Wang, 2001; Yu et al., 2018), soil respiration can also be facilitated by increases in temperature and soil moisture under climate change (Liu and Fang, 1997; Bauer et al., 2008; Trumbore and Czimczik, 2008). As a result, increased net photosynthesis leads to increased terrestrial O_2 production, but increased Rh leads to increased O_2 consumption. Because of these competing effects, it is difficult to determine whether terrestrial O_2 sources will increase, and quantitative analysis is needed.

Many studies have estimated terrestrial carbon sinks through variations in atmospheric O_2 content (Manning and Keeling, 2006; Tohjima et al., 2019; Li et al., 2021); however, to date, no studies have estimated terrestrial O_2 sources through carbon fluxes from the land. The limited availability of observations of oxidative ratios and net carbon fluxes have impeded the development of this type of study. Since 2010, many satellites, such as the Greenhouse gases Observing SATellite (GOSAT) and the Soil Moisture Active Passive (SMAP) satellite, have focused on monitoring the global carbon budget. However, the durations of the observational time periods from satellites are insufficient for analyzing the historical response of terrestrial O_2 sources to climate change. For example, SMAP net ecosystem exchange data cover only the years 2016 to 2019. *In situ* carbon flux observations, such as observations from the FLUXNET network, are both spatially scattered and temporally discontinuous, and thus, have difficulty exhibiting long-term variations and distribution features. Therefore, biochemical models that can simulate terrestrial carbon fluxes are considered when analyzing modern carbon and oxygen cycles. Several dynamic global vegetation models (DGVMs) and global ocean biogeochemical models have been used to estimate biotic and oceanic carbon sinks; they were utilized by the Global Carbon Project (GCP) to estimate the global carbon budget (Sitch et al., 2015; Friedlingstein et al., 2019). Here, we use the results of coupled climate models from the Sixth Coupled Model Intercomparison Project (CMIP6) to explore the changes in terrestrial O_2 sources in response to climate change and anthropogenic activities.

To compensate for the lack of previous studies on terrestrial O_2 sources, we integrated a globally gridded oxidative ratio database and provided a clear map of the current terrestrial O_2 sources. Additionally, this study shows how and why the main O_2 source regions will change in the future (Figure 1). Through this study, we highlight that as an important component of the modern oxygen cycle, terrestrial O_2 sources and their changes due to anthropogenic activities should be given ample attention.

2. Data and methods

2.1 Calculation of terrestrial O_2 production

The exchange of atmospheric O_2 with terrestrial ecosystems can be expressed in terms of the net carbon flux from the ecosystem to the atmosphere (the net ecosystem production, NEP, units: kg m^{-2}) and the net oxidative ratio (OR_{net}; a molar O_2 to CO_2 ratio, unit: mol mol^{-1}) (Keeling and Shertz, 1992) as follows:

$$F_{O_2} = \mathrm{OR}_{\mathrm{net}} \times \mathrm{NEP} \times \frac{M_{O_2}}{M_C}, \tag{1}$$

where F_{O_2} represents the O_2 flux between the atmosphere and the terrestrial biosphere (unit: kg m^{-2}). A positive F_{O_2} value indicates O_2 emitted into the atmosphere, and a negative value indicates O_2 absorbed from the atmosphere. Here, *NEP* is the net ecosystem production, defined as the net natural flux of carbon from the atmosphere to the land calculated as the difference between uptake associated with photosynthesis and the release of carbon from the sum of plant and soil respiration and natural fire. The oxidative ratio is the molar ratio of O_2 production to CO_2 consumption, or the ratio of O_2 consumption to CO_2 production, for a given process. It was first introduced in a study by Keeling (1988). For example, the globally averaged oxidative ratio of fossil fuel combustion is approximately 1.39±0.04 mol mol^{-1} (Bender et al., 1998) and each type of fossil fuel has its own typical oxidative ratio value (Liu et al., 2020). In our study, OR_{net} is defined as the ratio of net terrestrial O_2 production to the net terrestrial carbon sink. M_{O_2} and M_C are the molar masses of O_2 and carbon, and $M_{O_2}/M_C \approx 2.667$.

2.2 Integration of the global gridded OR_{net}

The overall chemical equations for the photosynthesis (2) and respiration processes (3) are as follows:

$$6CO_2+6H_2O \rightarrow C_6H_{12}O_6+6O_2 \tag{2}$$

$$C_6H_{12}O_6+6O_2 \rightarrow 6CO_2+6H_2O \tag{3}$$

Therefore, one mole of O_2 is emitted by the ecosystem, while one mole of CO_2 is absorbed (or vice versa), which means that in theory, OR_{net} should be 1.0 mol mol^{-1}(Huang et al., 2018). However, due to the existence of nitrogen (N) in plant shoots and other N-rich tissues, the observed OR_{net} values vary between 0.98 and 1.26 mol mol^{-1} (Bloom et al., 1989). The global averaged OR_{net} was estimated to be

https://engine.scichina.com/doi/10.1007/s11430-021-9956-5

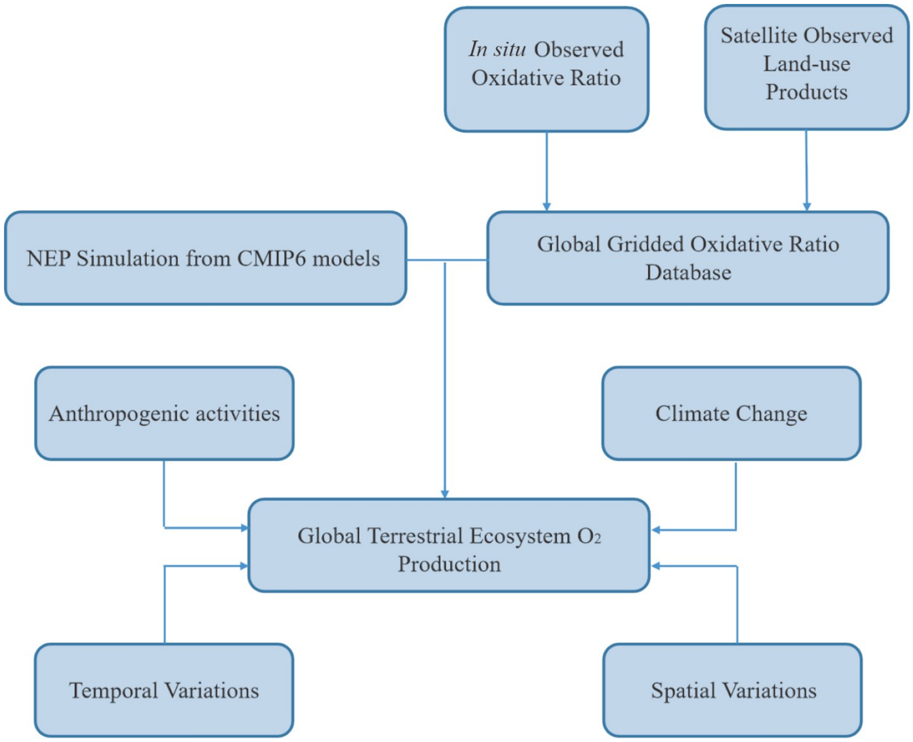

Figure 1 Illustration of the overall methodology and procedural steps of this study. Based on the *in situ* observed oxidative ratios and satellite land-use data, we integrated a long-term gridded, global oxidative ratio database. Combined with NEP simulations from CMIP6 models, we analyzed the temporal and spatial variation in terrestrial O_2 production. Then, based on land-use change and the competing effects of net photosynthesis and heterotrophic respiration, we explored the influence of anthropogenic activities and climate change on oxygen sources.

1.1 mol mol^{-1} based on the results of the Biosphere 2 experiment (Severinghaus, 1995), and this value has been used in various studies to estimate the terrestrial carbon sink (Keeling et al., 1996; Langenfelds et al., 1999; Battle et al., 2000; Manning and Keeling, 2006). However, additional *in situ* observations have shown that OR_{net} would change with plant types, environmental conditions and seasons (Seibt et al., 2004; Gallagher et al., 2017; Battle et al., 2019), implying that OR_{net} should not be set as a constant value when analyzing the spatial and temporal characteristics of terrestrial O_2 sources. Therefore, to analyze the temporal and spatial variations in the terrestrial O_2 sources, both a long-term global gridded OR_{net} database and a gridded NEP database are needed.

However, there is no such OR_{net} database available on a global scale. Previous observational studies have mainly focused on OR_{net} in North America, Europe, and Australia (Masiello et al., 2008; Gallagher et al., 2017). Using previous *in situ* observations and satellite-observed land-use data, we integrated a historical globally gridded OR_{net} database covering the years from 2001 to 2015 (Appendix Text S1, https://link.springer.com). The OR_{net} values from previous studies, their corresponding plant types, and the applied regional information are listed in Table 1. We applied these values to the corresponding locations in the grid. For the regions lacking *in situ* experiments, we used the average global OR_{net} values corresponding to the typical underlying surfaces from Clay and Worrall (2015), which are listed in Appendix Table S1. The OR_{net} value for unvegetated land was set as the default value. Land-use types for 2001–2015 were obtained from the Terra satellite Moderate Resolution Imaging Spectroradiometer (MODIS) products, which were acquired from the NASA Goddard Space Flight Center (http://ladsweb.nascom.nasa.gov/data/search.html). In this database, the terrain is identified as water, grassland, shrubs, broadleaf crops, savannah, evergreen broadleaf forests, deciduous broadleaf forests, evergreen needleleaf forests, deciduous needleleaf forests, unvegetated land, and urban, totalling 11 types. The original resolution of this land-use type data was 0.05°×0.05°, and after filling the grids with specific OR_{net} values, we interpolated the OR_{net} database to a 1.0°×1.0° resolution.

To estimate and analyze the future changes in the total amount of terrestrial O_2 sources and their distribution characteristics, we also need to develop an OR_{net} database under future projections according to the future land-use projections under different Shared Socioeconomic Pathways (SSPs). Here, we used fractional land-use patterns from the second Land-Use Harmonization (LUH2) project (Hurtt et al., 2020) to specify the future land-use types from 2015 to 2100. This database is also utilized by the Earth System Models in CMIP6. In the LUH2 database, land use is cate-

Table 1 OR_{net} values, corresponding plant types, and location information from previous studies

Oxidative ratio	Vegetation and observation location	Applied regions	Study information
1.30±0.05	Temperate grassland and forest, Kiel, Germany	54.25°–54.43°N, 10.03°–10.21°E	Dilly, 2001
1.11	Temperate native grassland, Giessen, Germany	50.52°–50.64°N, 8.55°–8.78°E	Müller et al., 2004
1.03±0.05	Deciduous forests, Massachusetts, USA	41°–43°N, 69°–73°W	Seibt et al., 2004
1.01±0.06	Evergreen needleleaf forests, Scotland, UK	54°–61°N, 0°–8°W	Seibt et al., 2004
1.08±0.16	Mixed forests, central Germany	49°–52°N, 7°–13°E	Seibt et al., 2004
0.99±0.01	Deciduous broad-leaved forests, central Germany	49°–52°N, 7°–13°E	Kozlova et al., 2005
2.1±0.2	Glaciers, Jungfraujoch, Switzerland	46.51°–46.56°N,7.90–8.00°E	Sturm et al., 2005
2.2±0.2	Snow and ice, Puy de Dome, France	45.29°–46.26°N, 2.39–3.98°E	Sturm et al., 2005
1.06±0.04	Mixed forest, northern Wisconsin, USA	42°–48°N, 86°–92°W	Stephens et al., 2007
1.00±0.03	Corn, Michigan, USA	41°–48°N, 82°–86°W	Masiello et al., 2008
1.07±0.04	Boreal black spruce forest, Alaska, USA	51°–72°N, 129°–170°W	Hockaday et al., 2009
1.06±0.04	Temperate Mediterranean woodland, Australia	10°–45°S, 100°–160°E	Hockaday et al., 2009
1.10±0.04	Subtropical woodland, Australia	10°–45°S, 100°–160°E	Hockaday et al., 2009
1.20±0.02	Temperate grassland, California, USA	32°–42°N, 114°–125°W	Hockaday et al., 2009
1.10±0.04	Temperate Mediterranean pasture, Australia	10°–45°S, 100°–160°E	Hockaday et al., 2009
0.96±0.04	Subtropical native grassland, Australia	10°–45°S, 100°–160°E	Hockaday et al., 2009
1.02±0.03	Deciduous broad-leaved forests, central Japan	30°–45°N, 129°–145°E	Ishidoya et al., 2013
1.030±0.001	Crops, Michigan, USA	41°–48°N, 82°–86°W	Gallagher et al., 2014
0.89±0.12	Evergreen forests, western Russia	50°–70°N, 28°–60°E	van der Laan et al., 2014
1.05	Evergreen forests, Swaziland and South Africa	20°–35°S, 10°–35°E	Clay and Worrall, 2015
1.08±0.03	Deciduous forests, Swaziland and South Africa	20°–35°S, 10°–35°E	Clay and Worrall, 2015
1.08±0.02	Croplands, Swaziland and South Africa	20°–35°S, 10°–35°E	Clay and Worrall, 2015
1.07±0.03	Grasslands, Swaziland and South Africa	20°–35°S, 10°–35°E	Clay and Worrall, 2015
1.11	Mixed forests, Swaziland and South Africa	20°–35°S, 10°–35°E	Clay and Worrall, 2015
1.10±0.02	Shrublands, Swaziland and South Africa	20°–35°S, 10°–35°E	Clay and Worrall, 2015
1.09	Savannas, Swaziland and South Africa	20°–35°S, 10°–35°E	Clay and Worrall, 2015
1.06±0.05	Woody savannas, Swaziland and South Africa	20°–35°S, 10°–35°E	Clay and Worrall, 2015
0.99±0.04	Permanent wetlands, Swaziland and South Africa	20°–35°S, 10°–35°E	Clay and Worrall, 2015
1.039±0.007	Deciduous broad-leaved forests, Tennessee, USA	35°–37°N, 81°–91°W	Hockaday et al., 2015
1.069±0.014	Coniferous forests, Michigan, USA	41°–48°N, 82°–86°W	Gallagher et al., 2017
1.039±0.006	Deciduous forests, Michigan, USA	41°–48°N, 82°–86°W	Gallagher et al., 2017
0.97±0.02	Peat land, northern England, UK	49°–56°N, 5°W–2°E	Worrall et al., 2017
1.081±0.007	Mixed deciduous forest, Massachusetts, USA	41°–43°N, 69°–73°W	Battle et al., 2019

gorized into C_3 annual crops, C_3 nitrogen-fixing crops, C_3 perennial crops, C_4 annual crops, C_4 perennial crops, pasture, rangeland, primary vegetation on forest land, primary vegetation on non-forest land, secondary vegetation on forest land, secondary vegetation on non-forest land and urban land, totaling 12 types. To remain consistent with the MODIS product, we merged all types related to crops into one "crop" type and merged "pasture" and "rangeland" into a "grassland" type. Then, we used the OR_{net} distribution for 2015 to estimate the global average value of each land-use type in LUH2; the specific values and their uncertainties are shown in Table S2. With these data, we completed the database of the future land-use projections and developed a database of future OR_{net} values under the SSP245 and SSP585 scenarios, covering the period from 2015 to 2100. To match the resolution of the historical OR_{net} database, the future OR_{net} was also linearly interpolated from a 0.25°×0.25° resolution to a 1.0°×1.0° resolution.

2.3 Terrestrial net carbon fluxes

According to eq. (1), NEP, which is the net carbon flux from terrestrial ecosystems, is also required to calculate terrestrial O_2 production. Satellite observations are of insufficient duration to analyze the long-term changes in terrestrial O_2 production, and *in situ* carbon flux observations are globally scattered and temporally discontinuous. Therefore, the results of the coupled models from CMIP6 were used in this study.

Several models from different institutes in CMIP6 couple with the biochemical module and hence can provide major terrestrial ecosystem fluxes (Eyring et al., 2016). The ensemble mean of the NEP results from the CMIP6 models was used in this study, which covers not only future projections (SSP245 and SSP585 for 2015–2100) but also the historical period (2001–2014). A historical experiment is a simulation of the recent past, and its input conditions are consistent with real historical observations. The SSP245 experiment is a modified Representative Concentration Pathway (RCP) scenario. In this scenario experiment, the models approximately follow the RCP4.5 global forcing pathway with SSP2 socioeconomic conditions, and the radiative forcing is projected to reach a level of 4.5 W m^{-2} in 2100. Similarly, the SSP585 experiment follows the RCP8.5 pathway with SSP5 socioeconomic conditions. SSP585 represents the worst-case scenario, whereas SSP245 is more optimistic. There are 15 models providing NEP data under the historical, SSP245, and SSP585 scenarios, but only 12 of them consider the nitrogen (N) cycle (Appendix Text S2). Therefore, these 12 models were used in this study and their detailed information is listed in Table 2. To explore the causes of future variations in terrestrial O_2 production, net primary production (NPP) and Rh simulation results from these CMIP6 models were also used in this study. In addition, because the CMIP6 models have different spatial resolutions, all the simulated fields were interpolated to a 1.0°×1.0° resolution to match the OR_{net} resolution.

To verify the ability of the CMIP6 model simulation to reproduce the changes in the terrestrial carbon sinks, we compared the simulated net carbon flux to the results of previous studies (shown in Figure 2a). NEP from the CMIP6 results shows that during the period from 2000 to 2014, approximately 2.52±0.04 Gt carbon per year was absorbed by the terrestrial ecosystem. This result is consistent with the most recently published terrestrial carbon sink in the GCP (http://www.globalcarbonproject.org) (Friedlingstein et al., 2019). In the GCP database, the terrestrial carbon sink is estimated through the ensemble mean of the results of various DGVMs participating in the "Trends and drivers of regional-scale sources and sinks of carbon dioxide" (TRENDY) project (Sitch et al., 2015), which represents a terrestrial sink of 2.91±0.60 Gt per year. We also considered the results of a satellite-driven Carnegie-Ames-Stanford Approach (CASA) biogeochemical model. NEP in the CASA model reached 2.30±0.58 Gt per year at the beginning of the 21st century. All three databases show an increasing NEP trend after 2000, which may be closely related to the increasing greenness of vegetation observed by satellites since the 1980s (Piao et al., 2020). The GOSAT satellite, which was launched in 2009, is the first spacecraft to measure the concentrations of CO_2 from space, and its observations are widely used for estimating the carbon budget (Yokota et al., 2009; Frankenberg et al., 2011; Chen et al., 2013). The global total amount of NEP from GOSAT is 2.70 ±0.29 Gt, which is close to that of CMIP6, 2.63±0.12 Gt during the period from 2010 to 2014, confirming that the CMIP6 models can well reproduce the global amount. Moreover, the GOSAT observations are in the range of the CMIP6 models simulation results (Figure 2a), which also proves the reliability of CMIP6 models.

Table 2 CMIP6 models used in this study to derive NEP, NPP and Rh and their information

Model	Institute	Land carbon component	Resolutions (latitude×longitude)
ACCESS-ESM1-5	Commonwealth Scientific and Industrial Research Organization, Australia	The CABLE land surface model with biogeochemistry (CASA-CNP) (CABLE2.4)	1.25°×1.875°
CESM2-WACCM	National Center for Atmospheric Research, USA	The Community Land Model Version 5 (CLM5)	0.9°×1.25°
CESM2	National Center for Atmospheric Research, USA	The Community Land Model Version 5 (CLM5)	0.9°×1.25°
CMCC-ESM2	Euro-Mediterranean Center on Climate Change, Italy	The Community Land Model Version 4.5 (CLM4.5)	0.9°×1.25°
CMCC-CM2-SR5	Euro-Mediterranean Center on Climate Change, Italy	The Community Land Model Version 4.5 (CLM4.5)	0.9°×1.25°
EC-Earth3-Veg-LR	European Centre of Medium Range Weather Forecast	The 2nd generation dynamic vegetation and biogeochemistry model LPJ-GUESS	0.7°×0.7°
EC-Earth3-CC	European Centre of Medium Range Weather Forecast	The 2nd generation dynamic vegetation and biogeochemistry model LPJ-GUESS	0.7°×0.7°
EC-Earth3-Veg	European Centre of Medium Range Weather Forecast	The 2nd generation dynamic vegetation and biogeochemistry model LPJ-GUESS	0.7°×0.7°
MPI-ESM-1-2-LR	Max Planck Institute for Meteorology, Germany	Jena Scheme for Biosphere-Atmosphere Coupling in Hamburg (JSBACH), Version 3.2	1.85°×1.875°
NorESM2-LM	Norwegian Climate Centre, Norway	The Community Land Model Version 5 (CLM5)	0.95°×1.875°
NorESM2-MM	Norwegian Climate Centre, Norway	The Community Land Model Version 5 (CLM5)	0.95°×2.5°
TaiESM1	Academia "Sinica", Taiwan Province, China	The Community Land Model Version 4.5 (CLM4.5)	0.95°×1.25°

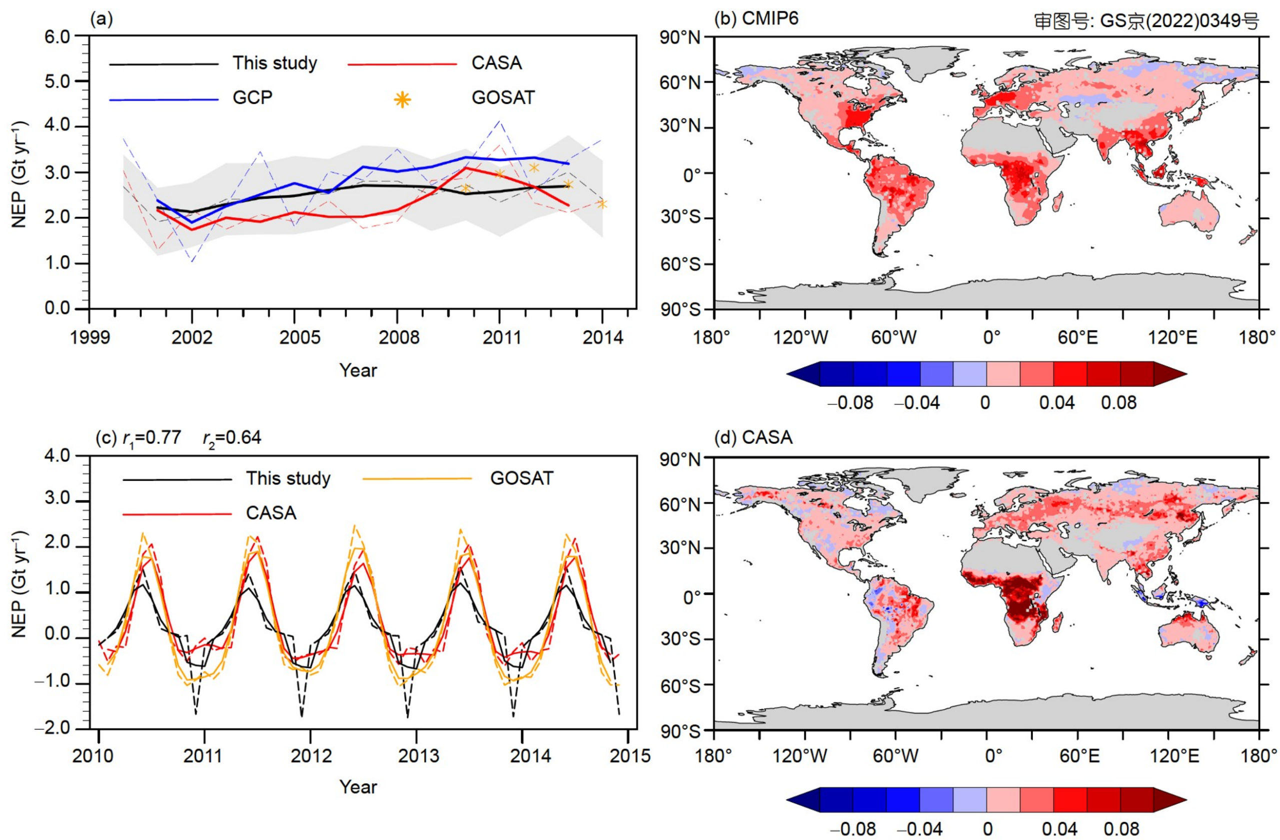

Figure 2 Comparison of net carbon fluxes among CMIP6 and previous studies. The dashed black, blue, red and orange lines denote the total global NEP from our study, GCP, CASA and GOSAT, respectively. The solid lines represent the 3-year (monthly) running means of the results. Orange asterisks represent the annual NEP from GOSAT. The correlation coefficient between CMIP6 and GOSAT is r_1, and between CMIP6 and CASA is r_2. Both correlation coefficients passed the 99% significance t test. (b) and (d) show the distribution of NEP from CMIP6 and CASA averaged from 2000 to 2014, in units of kg m^{-2}.

We also compared the seasonal variations in terrestrial carbon production among CMIP6 and other databases. As shown in Figure 2c, the amount of global terrestrial carbon production among three databases showed similar seasonal variations, although the amplitude of seasonal variation in CMIP6 models results is smaller. The correlation coefficient between CMIP6 and GOSAT is 0.77, and the correlation coefficient between CMIP6 and CASA also reaches 0.64 (both are significant at the 99% confidence level; a t test is used), indicating that the CMP6 models can also simulate the seasonal variation in NEP well.

The accuracy of the spatial distribution is critical to our study, and we compared the spatial distribution for NEP from the CMIP6 models and other databases (GCP only provides the global total value but doesn't provide the distribution). As shown in Figure 2b and 2d, the results show similar distribution patterns. Both figures show that the largest carbon sink exists in the tropics, especially in central Africa and areas of the Amazon. NEP decreases as latitude increases, and some terrestrial carbon sources are located in the boreal coastal regions. However, in the CMIP6 model results, NEP may be underestimated in the mid-latitudes, and the carbon sink in central Africa was also overlooked. Additionally, the CASA model shows large carbon sinks located in central and eastern Siberia. The CMIP6 model results also show similar distribution patterns to those of GOSAT for both annual and seasonal averages (Appendix Text S3; Appendix Figure S1). All these results confirm that the CMIP6 models can reproduce similar variations in the global total amount and regional patterns, suggesting that the CMIP6 model results are acceptable for deriving the terrestrial O_2 source distribution.

2.4 Explanation of future variations

As shown in eq. (1), the change in net carbon fluxes from terrestrial areas and the OR_{net} can both directly influence terrestrial O_2 sources. The net carbon flux can be represented as follows:

$$NEP = NPP - Rh, \tag{4}$$

NPP is the net primary production and Rh is the amount of heterotrophic respiration. Therefore, eq. (1) can be transformed into

$$F_{O_2} = OR_{net} \times (NPP - Rh). \tag{5}$$

Thus, we can conclude that the terrestrial O_2 source changes depend on the change in OR_{net} and the difference between the changes in NPP and Rh, i.e., ΔNPP−ΔRh. In our study, an OR_{net} database of future projections was derived from the projections of the LUH2 land-use models, which were mainly based on land-use changes. ΔNPP−ΔRh is derived from the CMIP6 models results, which were mainly based on climate change.

3. Results

3.1 The current terrestrial O_2 source

As mentioned in Section 2.1, the terrestrial O_2 source can be directly derived from OR_{net} and NEP. However, previous studies usually set the OR_{net} value to be a constant, and there has never been a long-term, global OR_{net} database. With the integrated OR_{net} global data in this study, we provide a clear map of the current distribution of the OR_{net} (shown in Figure 3a) for the first time. The uncertainty in the OR_{net} can be seen in Appendix Figure S2 and Appendix Text S4. The global area-weighted average OR_{net} is approximately 1.05±0.03 mol mol^{-1}, which is the same as that from Keeling and Manning (2014) and falls between the results of 1.06±0.06 mol mol^{-1} from Clay and Worrall (2015) and 1.04±0.03 mol mol^{-1} from Worrall et al. (2013). These similarities demonstrate that the results of our OR_{net} database are credible. Regional features reveal that the OR_{net} in the tropics, which are mainly covered by tropical savannahs, shrubs, and broadleaf forests, is larger than that at mid-latitudes, which are dominated by grass, and high latitudes, which are covered by needleleaf forests and open shrublands. Thus, there are wide variations in the OR_{net} among different regions, which demonstrates that the OR_{net} should not be considered a constant when discussing the distribution of terrestrial O_2 sources.

Furthermore, we obtained the current distribution of the global terrestrial O_2 sources. Figure 3b shows the global distribution of O_2 sources averaged from 2001 to 2014, and the values of terrestrial O_2 produced at different latitudes are summarized in Table 3. From the averaged results, we can see that the total amount of terrestrial O_2 production can reach 7.10±0.38 Gt per year, which shows that the terrestrial ecosystem is the primary source of atmospheric O_2 (global oceans only provide approximately 1.6 Gt per year according to the study of Li et al., 2020). The tropics (30°S–30°N) is the main O_2 source, providing approximately 4.78±0.30 Gt of O_2 yearly, or approximately 67.32% of the total terrestrial production. Furthermore, the Amazon forests, Central African forests, and Indonesian forests are the main sources within the tropics. The mid-latitudes (30°−60°S, 30°−60°N) provide approximately 2.23±0.16 Gt of O_2 (~31.41%) but show asymmetrical patterns between the two hemispheres due to land and sea distribution. The mid-latitudes in the

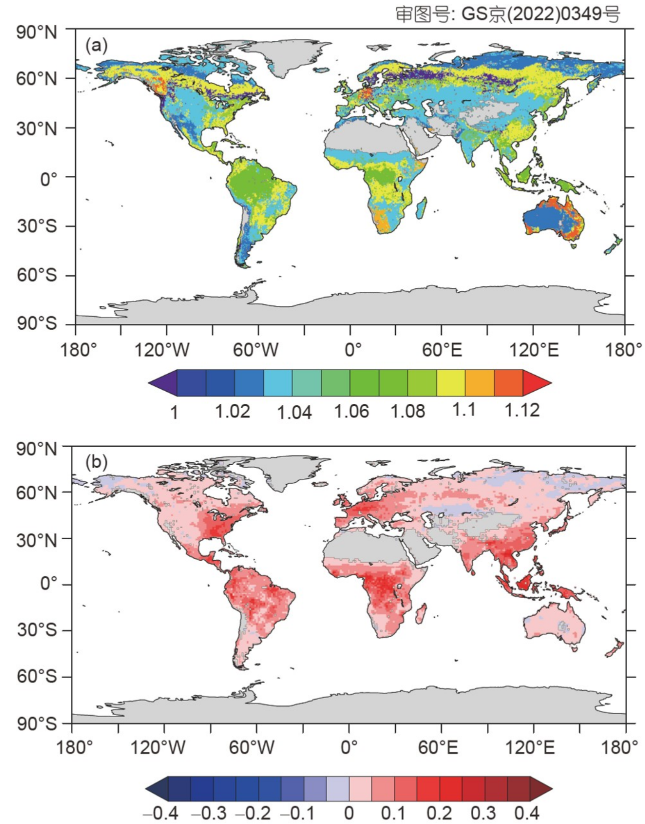

Figure 3 Current (average from 2001 to 2014) global distribution of (a) the OR_{net} and (b) terrestrial O_2 sources. The unit of OR_{net} is mol mol^{-1}, and the unit of the terrestrial O_2 source is kg m^{-2}.

Table 3 Amounts of terrestrial O_2 produced at different latitudes, averaged from 2001 to 2014

Regions	Average O_2 produced (Gt)
Tropics (30°S−30°N)	4.78±0.30 (67.32%)
South Mid-latitudes (30°−60°S)	0.18±0.03 (2.54%)
North Mid-latitudes (30°−60°N)	2.05±0.13 (28.87%)
North High-latitudes (60°−90°N)	0.09±0.06 (1.27%)
Total	7.10±0.38

Northern Hemisphere produce 2.05±0.13 Gt of O_2 per year, while those in the Southern Hemisphere produce only 0.18 ±0.03 Gt of O_2 per year. The two main mid-latitude O_2 sources are in eastern North America and western Europe. The high latitudes (60°S–90°S, 60°N–90°N), with low OR_{net} values and small net carbon fluxes, emit only 0.09±0.06 Gt (~1.27%) of O_2 into the atmosphere per year.

Figure 3b also shows that there are many regions where the O_2 fluxes are negative, which means that the ecosystems in these regions consume O_2 from the atmosphere instead of producing it. We defined these areas as "non-O_2-producing land", which appear not only in regions around the deserts in Central Asia but also in some boreal regions in the high latitudes of the Northern Hemisphere. The presence of non-

O_2-producing land informs that terrestrial ecosystems may not always be O_2 sources. Under climate change, a "global greening" phenomenon appears in the leaf area index and normalized difference vegetation index in various regions and implies an increase in vegetative growth (Jong et al., 2012). This phenomenon can be induced by a warming environment and be enhanced by the increased atmospheric CO_2 concentrations or by suitable land-use management, such as afforestation and the conversion of farmland to forests and grasslands (Chen et al., 2019). However, our study shows that there are currently many non-O_2-producing areas. This disrupts terrestrial O_2 production and should be considered in assessments of ecosystem health.

3.2 Future changes in terrestrial O_2 sources

Since the 1850s, considerable quantities of greenhouse gases have been emitted into the atmosphere due to industrialization, and these emissions have caused severe global climate change over the last century. In the future, anthropogenic activities, such as fossil fuel combustion and land-use change, will further influence ecosystems directly and indirectly. In this study, we utilized the CMIP6 model-simulated net carbon fluxes, and OR_{net} derived from land-use models to estimate the future effects of human activities and related climate change on terrestrial O_2 sources. Figure 4a shows the temporal variation in the global total amount of terrestrial O_2 sources from 2001 to 2100. Terrestrial O_2 sources showed a significant increase both during the historical period and in future projections. The ensemble mean of the CMIP6 models reveals that, by 2100, the amount of terrestrial O_2 emitted will increase from the current value of 7.10±0.38 to 7.51±0.27 under the SSP245 scenario or to 10.23±0.28 Gt under the SSP585 scenario. As shown by the decadal variations in Figure 4b, terrestrial O_2 production will increase until the 2050s, when fossil fuel combustion decreases in this projection, implying that terrestrial O_2 production is sensitive to anthropogenic activities. In contrast, terrestrial O_2 production under the SSP585 scenario will continue to increase in response to extreme anthropogenic activities.

Moreover, we analyzed changes in the global distribution of O_2 sources under the two different scenarios, and there were evident differences between them, as shown in Figure 5. In the future, the distribution of terrestrial O_2 sources will likely follow a scenario where more oxygen is produced from the mid-low latitudes, while the high latitudes become larger oxygen sinks (Figure 5c and 5d). Under the SSP245 scenario (Figure 5a), the Amazon forests, one of the main O_2 sources, will experience a reduction. Meanwhile, O_2 sources in the midlatitudes, such as eastern North America and western Europe, will also decrease. The non-O_2-producing land on the boreal coasts will show worse outcomes, removing more O_2 from the atmosphere than that during the historical period. The main increases will occur in eastern South America, central Africa, eastern Europe, and eastern and southern Asia. Under the RCP8.5 scenario (Figure 5b), production will increase nearly worldwide, except at the high latitudes. Decreases will only occur in northern Europe and in the northern coastal regions of Canada. It is difficult to explain all these changes, including those in the global total amount and distribution, because they could be caused by human activities, such as land-use changes, or by climate change, such as changes in temperature, precipitation, and CO_2 concentration. Here, we attempt to determine the dominant factor.

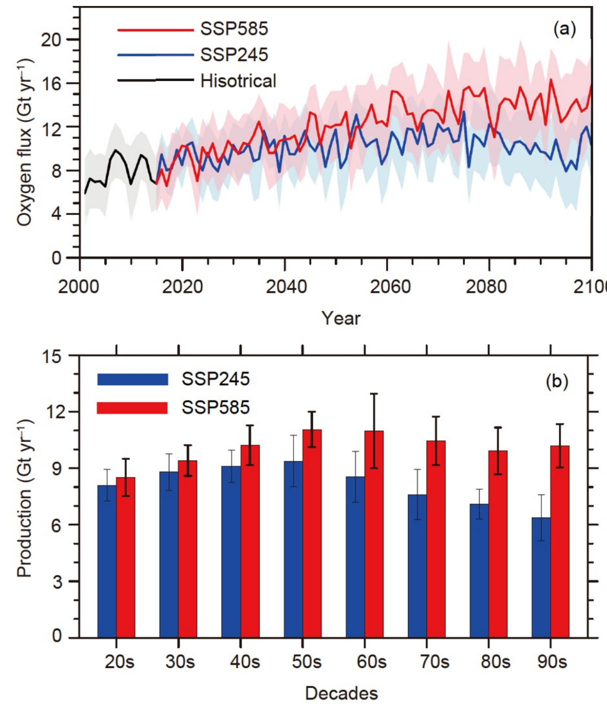

Figure 4 (a) Temporal variation in terrestrial O_2 sources and (b) its decadal variation in the 21st century. The black, blue, and red lines represent the ensemble mean of the models from the historical, SSP245, and SSP585 scenarios, respectively. The shading denotes the 95% confidence interval of the models. The blue and red bars represent the annual terrestrial O_2 production per decade in the SSP245 and SSP585 scenarios, respectively. The black lines denote the standard errors of the bars.

3.3 Explanations of future change

Here, according to the methods introduced in Section 2.4, we explain the future variations in terrestrial O_2 sources through the changes in OR_{net} and the difference between the changes in NPP and Rh, i.e., ΔNPP−ΔRh.

Figure 6a shows the change in the global average OR_{net} under the SSP245 and SSP585 scenarios, and it shows that the OR_{net} will decrease in the future. This result is ecologically plausible because, with a larger population, humans are likely to plant more crops, and herbaceous crops usually

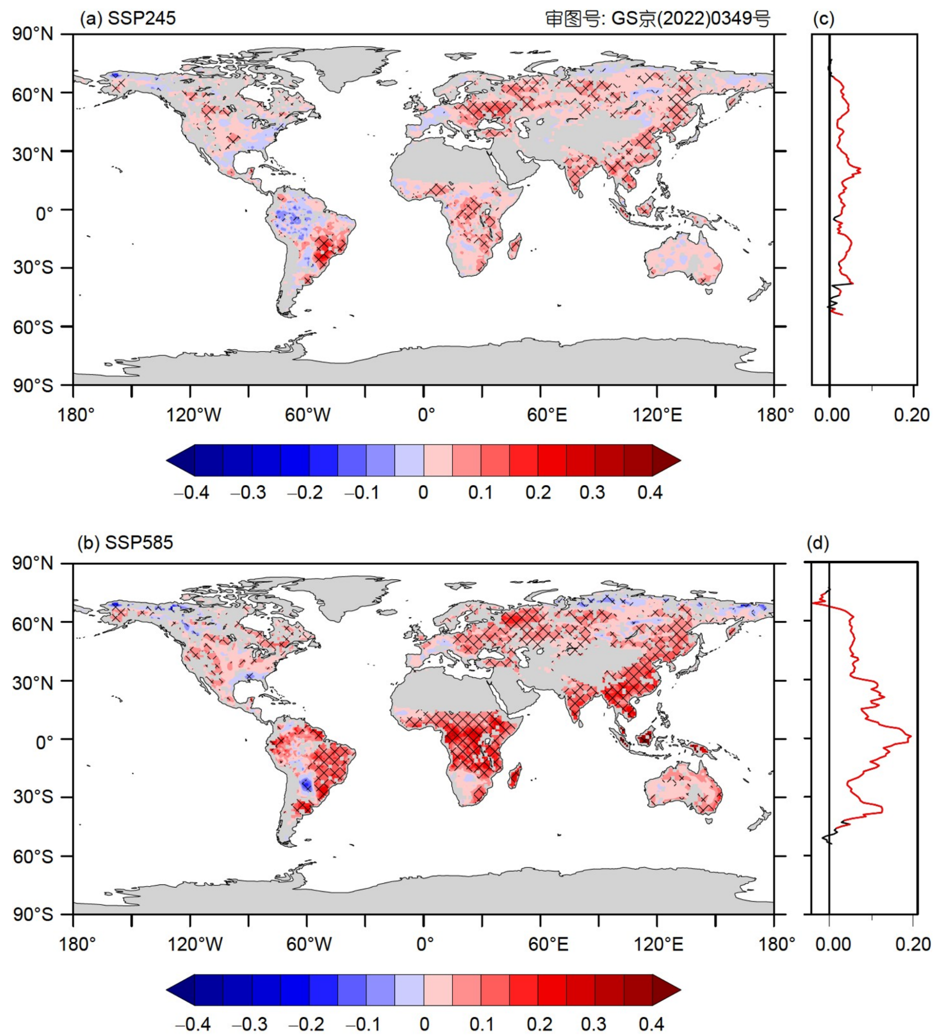

Figure 5 Changes in terrestrial O_2 sources under the (a) SSP245 and (b) SSP585 scenarios and their zonal means (c) and (d). The figures show the difference between the future O_2 sources (averaged from 2087 to 2100) and the current O_2 source (average from 2001 to 2014) in units of kg m^{-2}. The shaded areas in (a) and (b) are significant at the 95% confidence level. The thick red lines in Figure (c) and (d) denote the values that passed the 90% significance *t* test.

have lower OR_{net} than woody plants (Poorter and Villar, 1997). However, the decrease in the OR_{net} is small and occurs slowly, which is contrary to the increased terrestrial O_2 source. According to our results, OR_{net} will experience a decrease of only 0.001 mol mol^{-1}, which is much smaller than the decline of 0.01 mol mol^{-1} per century determined by Randerson et al. (2006); this can induce only slight variations in the terrestrial O_2 sources. Therefore, we conclude that the change in the total global amount of O_2 sources mainly arises from the difference between the changes in NPP and Rh (shown in Figure 6b). The variations in ΔNPP−ΔRh are similar to the variations in the O_2 sources. This value also shows a drastic and continuous increase under the SSP585 scenario, while the SSP245 scenario shows a smaller increase in ΔNPP−ΔRh after the 2050s than that in the previous 50 years.

As concluded in previous studies that used the LPJ model and CMIP5 models, increased CO_2 and temperature are beneficial for plant growth and cause strong net photosynthetic processes at both global and regional scales (Sun and Mu, 2013; Wang et al., 2014; Zhu et al., 2018). Rh also increases with increasing soil temperature and moisture, as shown *in situ* observations and analyses through the Conditional nonlinear optimal perturbation related to parameter (CNOP-P) method (Zhou et al., 2013; Sun and Mu, 2017; Francioni et al., 2019), and more O_2 is consumed. Our results from CMIP6 (Figure S3) can be mutually confirmed to the conclusions derived from the other analysis methods. Our study also finds that although the positive effects of climate change and CO_2 concentration on net photosynthesis will generally increase (Appendix Text S5), the variations in the trend under the SSP245 scenario imply that the response in soil respiration may be stronger (Figure 6b, blue bars), leading to disturbances in the carbon and oxygen cycles. Variations in soil respiration are often overlooked when discussing the effects of anthropogenic activities and related

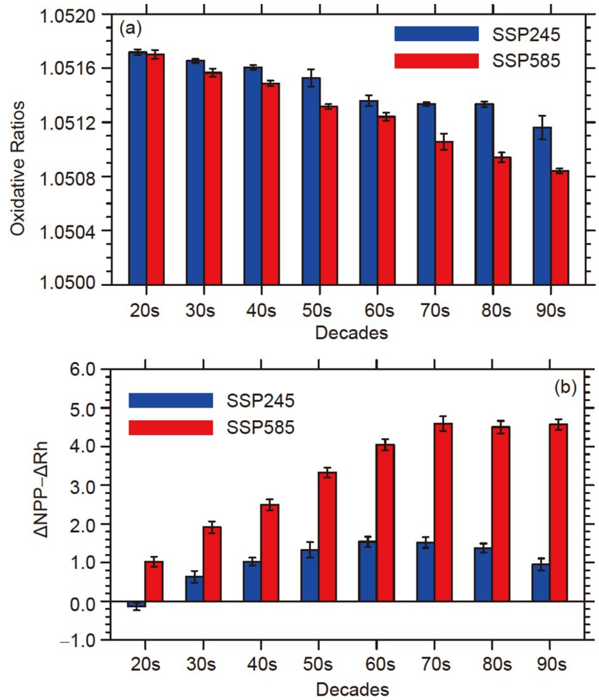

Figure 6 Decadal variations in (a) biotic OR_{net} and (b) ΔNPP−ΔRh in the future projections. The blue and red bars represent the results under the SSP245 and SSP585 scenarios, respectively. The black lines denote the standard errors of the bars.

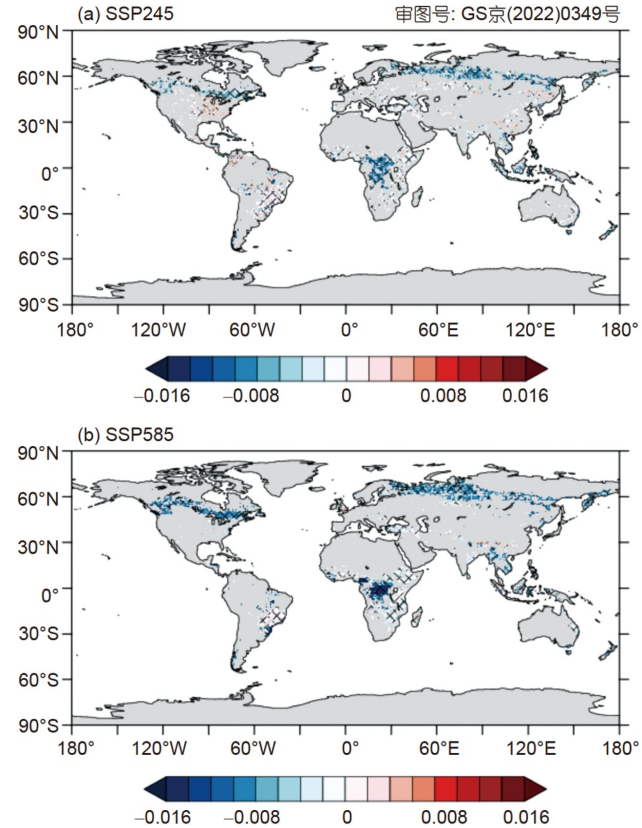

Figure 7 Changes in the terrestrial biotic OR_{net} under the (a) SSP245 and (b) SSP585 scenarios. The figures show the difference between the future distribution of OR_{net} (averaged from 2087 to 2100) and the current OR_{net} (average from 2001 to 2014) in units of mol mol^{-1}. A missing value represents no change in the future scenarios, or a missing OR_{net} value. The shading areas are significant at the 90% confidence level.

climate change on ecosystems, but our results indicate that they should be considered when evaluating land-use strategies and changing climatic conditions.

Compared with the change in the total global amount, variations in regional terrestrial O_2 sources are easily affected by many factors. As shown in Figure 7a and 7b, a major decrease in the OR_{net} occurs at high latitudes, especially at approximately 60°N. According to the land-use change in LUH2, this region is mainly covered by primary forest vegetation, which will become secondary forest vegetation (seen in Appendix Figure S4, Appendix Text S6). Therefore, vegetation in these regions is highly sensitive to climate change, which corresponds to the results of previous studies (Raich and Schlesinger, 1992). As shown in Appendix Table S2, the OR_{net} of the secondary vegetation is smaller than that of the primary vegetation. Another evident decrease occurs in central Africa, where the dominant vegetation is currently forest, which will be transformed into mixed forests consisting of grassland, primary non-forest vegetation, and secondary forest vegetation under future projections. The impact of human activities is evident in this region, and the OR_{net} decreases by approximately 0.01 mol mol^{-1}. Increases mainly occur in eastern South America, where vegetation transforms from grassland to crops (Appendix Text S6), inducing a slight increase of 0.001 mol mol^{-1}. This increase does not compensate for the decreases at the high latitudes and in central Africa, which ultimately lead to an overall decrease in the average global OR_{net}.

Figure 8a and 8b compare the changes in NPP and Rh under the SSP245 and SSP585 scenarios, respectively. We found that the increase in Rh can exceed that of the NPP in various regions under the SSP245 scenario, which explains why several regions experience a decline in O_2 production. The greatest decline occurs in the Amazon forests, potentially owing to more frequent droughts in the future (IPCC AR5 Report, 2013). Amazon forests are sensitive to precipitation levels. When the eastern Amazon forests experience drought, reduced plant growth also leads to decreased evapotranspiration; hence, the vapor transported to the western forests decreases. Thus, the net photosynthesis throughout the Amazon forests decreases through this positive feedback. However, the abundant soil moisture and increased temperature ensure that soil respiration will continue to increase in the future, which explains why the increase in Rh exceeds that of the NPP by the end of the 21st century. Overall, this change causes a decline in O_2 production in the Amazon forests.

High latitudes are another region that should be con-

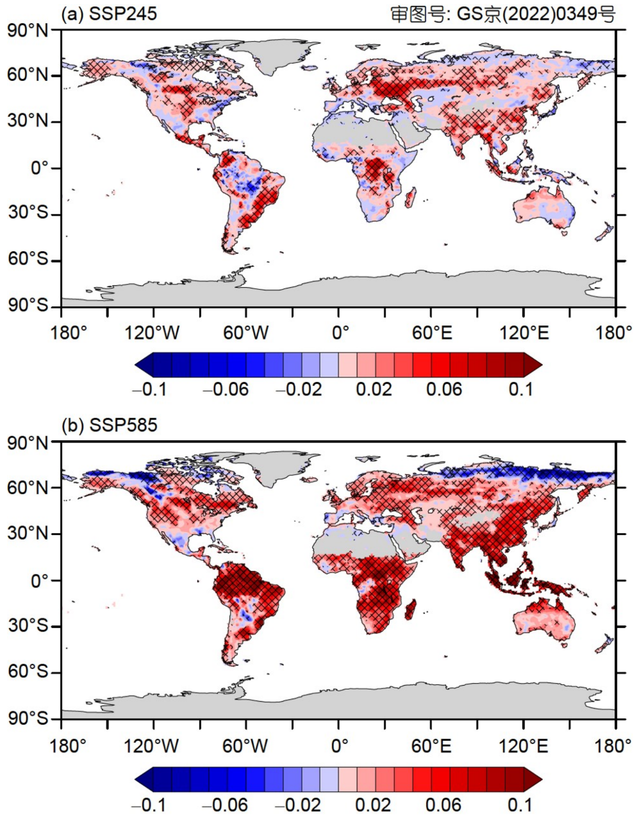

Figure 8 Change under ΔNPP−ΔRh in the (a) SSP245 and (b) SSP585 scenarios. The figures show the difference between the future distribution of ΔNPP−ΔRh (averaged from 2086 to 2100) and initial ΔNPP−ΔRh (average from 2015 to 2029) in units of kg m^{-2}. The shaded areas are significant at the 95% confidence level.

sidered, such as the northern regions of North America, northern Europe, and Siberia. As shown in Figure 8, Rh increases sharply in the projections, partly owing to a phenomenon called "Arctic amplification," in which the temperatures at high latitudes in the Northern Hemisphere show a dramatic increase under climate change (Cusbasch et al., 2001; Braganza et al., 2003, 2004). The increased soil temperatures, accompanied by the melting of snow and ice, result in increases in soil moisture, which leads to an increase in Rh. Combined with the decrease in OR_{net} mentioned above, high latitudes will experience a severe decline in terrestrial O_2 sources in the future.

4. Discussions

The results show that land will provide more O_2 in the future than during any other historical period. However, we must stress that this situation is still not optimistic because the amount of O_2 consumed due to fossil fuel combustion is also increasing to unprecedented levels. A previous study showed that fossil fuel combustion increased from 1.99 to 29.76 Gt per year from 1900 to 2005 (Huang et al., 2018). Enhanced terrestrial O_2 production still cannot compensate for this loss of atmospheric O_2; therefore, the decline in atmospheric O_2 concentration is accelerating (Valentino et al., 2008; Sirignano et al., 2010). Additionally, land-use changes, which can result from deforestation, excessive grazing, and excessive cultivation, influence O_2 production by changing the OR_{net}. Therefore, if we rely solely on ecosystem adaptation and recovery and do not reduce or limit fuel combustion and other anthropogenic activities, the O_2 concentration will continue to decline.

Our study also shows the distribution of current terrestrial O_2 sources for the first time. This distribution also reveals non-O_2-producing land, which exists not only in the regions around deserts but also worldwide. In regions near deserts, desertification, which refers to the accelerated expansion of deserts and arid land under climate change (Huang et al., 2016), will restrain net photosynthesis and lead to decreases in regional O_2 production. At high latitudes, the vegetation type is the main cause of non-O_2-producing land. The O_2 produced from evergreen and deciduous, coniferous forests through net photosynthesis is usually overestimated and is much less than that from tropical vegetation (Fang et al., 2006). Therefore, in the future, the distribution of terrestrial O_2 sources will likely follow a scenario where more O_2 will be emitted from the tropics, but the O_2 produced at the high latitudes will decrease.

Our study derived terrestrial O_2 sources from terrestrial net carbon fluxes. In contrast with studies estimating carbon sinks from the change in atmospheric O_2 concentration, which usually set OR_{net} as a constant, we developed a global gridded OR_{net} database, which can reproduce the long-term variations and regional characteristics of OR_{net}. Our results show that the current global average OR_{net} can reach 1.05 mol mol^{-1}, which is close to the latest results (Worrall et al., 2013; Clay and Worrall, 2015). In addition, in recent studies (Tohjima et al., 2019; Li et al., 2020), the biotic OR_{net} was 1.10 mol mol^{-1}, which is based on the soil respiration oxidative ratio from the Biosphere 2 experiment (Severinghaus, 1995). Our results demonstrate that changes in land use can result in variations in the OR_{net} (see Figure 6a). Human activities have extensively modified the vegetation cover over the past 20 years, and OR_{net} values should be updated accordingly. Additionally, improvements in observation methods and instruments that allow for the utilization of the latest field observations lead to better estimates for OR_{net}.

However, shortcomings are evident in our OR_{net} database. First, the field observations used in this study were mainly located in North America, Europe, Africa, and Australia. There were almost no such observations collected from South America and central and eastern Asia. For some important regions, such as the Amazon forests, which are thought to be the primary carbon sinks and O_2 sources, we could only utilize the global average OR_{net} values of typical plants. This method may induce a large bias when estimating the contribution of each region. Another deficiency is that observations from arid and alpine regions are limited. In our study, the OR_{net} values in the desert and polar areas were set as missing values. Although vegetation coverage is sparse in these areas, arid lands occupy approximately 14.9% of the global land area (Huang et al., 2016), and their contributions to the modern carbon and oxygen cycle should be considered.

5. Conclusions

In this study, based on a land-use database and previously observed OR_{net}, we integrated a novel long-term global gridded OR_{net} database. Combined with net carbon fluxes, we obtained the current terrestrial O_2 source distribution. Currently, the land on Earth can produce approximately 7.10 ±0.38 Gt of oxygen per year. The tropics are the main source of atmospheric O_2 and produce approximately 4.78±0.30 Gt of O_2 per year. The midlatitudes provide approximately 2.23 ±0.16 Gt of O_2 yearly, and two major O_2 sources, eastern North America and western Europe, are in the midlatitudes. Long-term analysis reveals that terrestrial oxygen sources are sensitive to anthropogenic activities and climate changes. The future variations in terrestrial oxygen sources will likely follow a scenario where more oxygen will be produced in the low-middle latitudes, while the high latitudes will become larger oxygen sinks. Through this study, we provide a better understanding of terrestrial ecosystem oxygen-producing processes, which supplement modern oxygen cycle studies. Additionally, the analysis of drivers for variations in oxygen sources can be used to couple the oxygen cycle into Earth System Models (ESMs) to estimate future atmospheric oxygen levels.

Acknowledgements *The authors acknowledge the World Climate Recruitment Programme's Working Group on Coupled Modelling and the Global Organization for Earth System Science Portals for producing the CMIP6 model simulations and making them available for analysis. They can be downloaded at https://esgf-node.llnl.gov/search/cmip6/. The carbon flux database from the GFED4 database can be downloaded from https://daac.ornl.gov/VEGETATION/guides/fire_emissions_v4.html. This work was jointly supported by the National Natural Science Foundation of China (Grant Nos. 41521004 and 41991231), the China University Research Talents Recruitment Program (Grant No. B13045) and the Fundamental Research Funds for the Central Universities (Grant Nos. lzujbky-2021-kb12 and lzujbky-2021-63).*

References

Battle M, Bender M L, Tans P P, White J W C, Ellis J T, Conway T, Francey R J. 2000. Global carbon sinks and their variability inferred from atmospheric O_2 and $\delta^{13}C$. Science, 287: 2467–2470

Battle M O, Munger J W, Conley M, Sofen E, Perry R, Hart R, Davis Z, Scheckman J, Woogerd J, Graeter K, Seekins S, David S, Carpenter J. 2019. Atmospheric measurements of the terrestrial O_2:CO_2 exchange ratio of a midlatitude forest. Atmos Chem Phys, 19: 8687–8701

Bauer J, Herbst M, Huisman J A, Weihermüller L, Vereecken H. 2008. Sensitivity of simulated soil heterotrophic respiration to temperature and moisture reduction functions. Geoderma, 145: 17–27

Bender M L, Battle M, Keeling R F. 1998. The O_2 balance of the atmosphere: A tool for studying the fate of fossil-fuel CO_2. Annu Rev Energy Environ, 23: 207–223

Bloom A J, Caldwell R M, Finazzo J, Warner R L, Weissbart J. 1989. Oxygen and carbon dioxide fluxes from barley shoots depend on nitrate assimilation. Plant Physiol, 91: 352–356

Braganza K, Karoly D J, Hirst A C, Mann M E, Stott P, Stouffer R J, Tett S F B. 2003. Simple indices of global climate variability and change: Part I: Variability and correlation structure. Clim Dyn, 20: 491–502

Braganza K, Karoly D J, Hirst A C, Stott P, Stouffer R J, Tett S F B. 2004. Simple indices of global climate variability and change part II: Attribution of climate change during the twentieth century. Clim Dyn, 22: 823–838

Chameides W L, Perdue M. 1997. Global Biogeochemical Cycles: A Computer-Interactive Study of Earth System. New York: Oxford University Press. 1–28

Chen C, Park T, Wang X, Piao S, Xu B, Chaturvedi R K, Fuchs R, Brovkin V, Ciais P, Fensholt R, Tømmervik H, Bala G, Zhu Z, Nemani R R, Myneni R B. 2019. China and India lead in greening of the world through land-use management. Nat Sustain, 2: 122–129

Chen Z, Yu G, Ge J, Sun X, Hirano T, Saigusa N, Wang Q, Zhu X, Zhang Y, Zhang J, Yan J, Wang H, Zhao L, Wang Y, Shi P, Zhao F. 2013. Temperature and precipitation control of the spatial variation of terrestrial ecosystem carbon exchange in the Asian region. Agric For Meteorol, 182-183: 266–276

Clay G D, Worrall F. 2015. Oxidative ratio (OR) of Southern African soils and vegetation: Updating the global OR estimate. Catena, 126: 126–133

Cusbasch U, Meehl G A, Boer G J, Stouffer R J, Dix M R, Noda A, Senior C A, Raper S, Yap K S. 2001. Climate Change 2001: The Scientific Basis: Contribution of Working Group I to The Third Assessment Report of The Intergovernmental Panel on Climate Change. New York: Cambridge University Press. 525–582

Dilly O. 2001. Microbial respiratory quotient during basal metabolism and after glucose amendment in soils and litter. Soil Biol Biochem, 33: 117–127

Eyring V, Bony S, Meehl G A, Senior C A, Stevens B, Stouffer R J, Taylor K E. 2016. Overview of the coupled model intercomparison project phase 6 (CMIP6) experimental design and organization. Geosci Model Dev, 9: 1937–1958

Fang J, Brown S, Tang Y, Nabuurs G J, Wang X, Shen H. 2006. Overestimated biomass carbon pools of the northern mid- and high latitude forests. Clim Change, 74: 355–368

Francioni M, D'Ottavio P, Lai R, Trozzo L, Budimir K, Foresi L, Kishimoto-Mo A W, Baldoni N, Allegrezza M, Tesei G, Toderi M. 2019. Seasonal soil respiration dynamics and carbon-stock variations in mountain permanent grasslands compared to arable lands. Agriculture, 9: 165

Frankenberg C, Fisher J B, Worden J, Badgley G, Saatchi S S, Lee J E, Toon G C, Butz A, Jung M, Kuze A, Yokota T. 2011. New global observations of the terrestrial carbon cycle from GOSAT: Patterns of plant fluorescence with gross primary productivity. Geophys Res Lett, 38: L17706

Friedlingstein P, Jones M W, O'Sullivan M, Andrew R M, Hauck J, Peters G P, Peters W, Pongratz J, Sitch S, Le Quéré C, Bakker D C E, Canadell J G, Ciais P, Jackson R B, Anthoni P, Barbero L, Bastos A, Bastrikov V, Becker M, Bopp L, Buitenhuis E, Chandra N, Chevallier F, Chini L P, Currie K I, Feely R A, Gehlen M, Gilfillan D, Gkritzalis T, Goll D S, Gruber N, Gutekunst S, Harris I, Haverd V, Houghton R A, Hurtt G, Ilyina T, Jain A K, Joetzjer E, Kaplan J O, Kato E, Klein Goldewijk K, Korsbakken J I, Landschützer P, Lauvset S K, Lefèvre N, Lenton A, Lienert S, Lombardozzi D, Marland G, McGuire P C, Melton J R, Metzl

N, Munro D R, Nabel J E M S, Nakaoka S I, Neill C, Omar A M, Ono T, Peregon A, Pierrot D, Poulter B, Rehder G, Resplandy L, Robertson E, Rödenbeck C, Séférian R, Schwinger J, Smith N, Tans P P, Tian H, Tilbrook B, Tubiello F N, van der Werf G R, Wiltshire A J, Zaehle S. 2019. Global carbon budget 2019. Earth Syst Sci Data, 11: 1783–1838

Gallagher M E, Masiello C A, Hockaday W C, Baldock J A, Snapp S, McSwiney C P. 2014. Controls on the oxidative ratio of net primary production in agricultural ecosystems. Biogeochemistry, 121: 581–594

Gallagher M E, Liljestrand F L, Hockaday W C, Masiello C A. 2017. Plant species, not climate, controls aboveground biomass O_2:CO_2 exchange ratios in deciduous and coniferous ecosystems. J Geophys Res-Biogeosci, 122: 2314–2324

Han D, Huang J, Ding L, Liu X, Li C, Yang F. 2021. Oxygen footprint: An indicator of the anthropogenic ecosystem changes. Catena, 206: 105501

Hockaday W C, Masiello C A, Randerson J T, Smernik R J, Baldock J A, Chadwick O A, Harden J W. 2009. Measurement of soil carbon oxidation state and oxidative ratio by ^{13}C nuclear magnetic resonance. J Geophys Res, 114: G02014

Hockaday W C, Gallagher M E, Masiello C A, Baldock J A, Iversen C M, Norby R J. 2015. Forest soil carbon oxidation state and oxidative ratio responses to elevated CO_2. J Geophys Res-Biogeosci, 120: 1797–1811

Huang J, Huang J, Liu X, Li C, Ding L, Yu H. 2018. The global oxygen budget and its future projection. Sci Bull, 63: 1180–1186

Huang J, Liu X, He Y, Shen S, Hou Z, Li S, Li C, Yao L, Huang J. 2021. The oxygen cycle and a habitable Earth. Sci China Earth Sci, 64: 511–528

Huang J, Yu H, Guan X, Wang G, Guo R. 2016. Accelerated dryland expansion under climate change. Nat Clim Change, 6: 166–171

Hurtt G C, Chini L, Sahajpal R, Frolking S, Bodirsky B L, Calvin K, Doelman J C, Fisk J, Fujimori S, Klein Goldewijk K, Hasegawa T, Havlik P, Heinimann A, Humpenöder F, Jungclaus J, Kaplan J O, Kennedy J, Krisztin T, Lawrence D, Lawrence P, Ma L, Mertz O, Pongratz J, Popp A, Poulter B, Riahi K, Shevliakova E, Stehfest E, Thornton P, Tubiello F N, van Vuuren D P, Zhang X. 2020. Harmonization of global land use change and management for the period 850–2100 (LUH2) for CMIP6. Geosci Model Dev, 13: 5425–5464

Ishidoya S, Murayama S, Takamura C, Kondo H, Saigusa N, Goto D, Morimoto S, Aoki N, Aoki S, Nakazawa T. 2013. O_2:CO_2 exchange ratios observed in a cool temperate deciduous forest ecosystem of central Japan. Tellus B-Chem Phys Meteorol, 65: 21120

Jong R, Verbesselt J, Schaepman M E, Bruin S. 2012. Trend changes in global greening and browning: Contribution of short-term trends to longer-term change. Glob Change Biol, 18: 642–655

Keeling R F. 1988. Measuring correlations between atmospheric oxygen and carbon dioxide mole fractions: A preliminary study in urban air. J Atmos Chem, 7: 153–176

Keeling R F, Shertz S R. 1992. Seasonal and interannual variations in atmospheric oxygen and implications for the global carbon cycle. Nature, 358: 723–727

Keeling R F, Piper S C, Heimann M. 1996. Global and hemispheric CO_2 sinks deduced from changes in atmospheric O_2 concentration. Nature, 381: 218–221

Keeling R F, Manning A C. 2014. Treatise on Geochemistry. 2nd ed. Amsterdam: Elsevier. 385–404

Kozlova E A, Manning A C, Jordan A, Brand W. 2005. Investigations of the land biotic O_2:CO_2 exchange ratios in photosynthesis and respiration. Seoul: Proceedings of the 7th International Carbon Dioxide Conference

Langenfelds R L, Francey R J, Steele L P, Battle M, Keeling R F, Budd W F. 1999. Partitioning of the global fossil CO_2 sink using a 19-year trend in atmospheric O_2. Geophys Res Lett, 26: 1897–1900

Li C, Huang J, Ding L, Liu X, Yu H, Huang J. 2020. Increasing escape of oxygen from oceans under climate change. Geophys Res Lett, 47: e86345

Li C, Huang J, Ding L, Liu X, Han D, Huang J. 2021. Estimation of oceanic and land carbon sinks based on the most recent oxygen budget. Earths Future, 9: e02124

Liu S, Fang J. 1997. Effect factors of soil respiration and the temperature's effects of soil respiration in the global scale (in Chinese). Acta Ecologica Sinica, 17: 469–476

Liu X, Huang J, Huang J, Li C, Ding L, Meng W. 2020. Estimation of gridded atmospheric oxygen consumption from 1975 to 2018. J Meteorol Res, 34: 646–658

Maltepe E, Saugstad O D. 2009. Oxygen in health and disease: Regulation of oxygen homeostasis-clinical implications. Pediatr Res, 65: 261–268

Manning A C, Keeling R F. 2006. Global oceanic and land biotic carbon sinks from the scripps atmospheric oxygen flask sampling network. Tellus B-Chem Phys Meteorol, 58: 95–116

Masiello C A, Gallagher M E, Randerson J T, Deco R M, Chadwick O A. 2008. Evaluating two experimental approaches for measuring ecosystem carbon oxidation state and oxidative ratio. J Geophys Res, 113: G03010

Müller C, Abbasi M K, Kammann C, Clough T J, Sherlock R R, Stevens R J, Jäger H J. 2004. Soil respiratory quotient determined via barometric process separation combined with nitrogen-15 labeling. Soil Sci Soc Am J, 68: 1610–1615

Nemani R R, Keeling C D, Hashimoto H, Jolly W M, Piper S C, Tucker C J, Myneni R B, Running S W. 2003. Climate-driven increases in global terrestrial net primary production from 1982 to 1999. Science, 300: 1560–1563

Piao S, Friedlingstein P, Ciais P, Viovy N, Demarty J. 2007. Growing season extension and its impact on terrestrial carbon cycle in the Northern Hemisphere over the past 2 decades. Glob Biogeochem Cycle, 21: GB3018

Piao S, Wang X, Park T, Chen C, Lian X, He Y, Bjerke J W, Chen A, Ciais P, Tømmervik H, Nemani R R, Myneni R B. 2020. Characteristics, drivers and feedbacks of global greening. Nat Rev Earth Environ, 1: 14–27

Poorter H, Villar R. 1997. Plant Resource Allocation. Hague: SPB Academic. 39–72

Raich J W, Schlesinger W H. 1992. The global carbon dioxide flux in soil respiration and its relationship to vegetation and climate. Tellus B-Chem Phys Meteorol, 44: 81–99

Randerson J T, Masiello C A, Still C J, Rahn T, Poorter H, Field C B. 2006. Is carbon within the global terrestrial biosphere becoming more oxidized? Implications for trends in atmospheric O_2. Glob Change Biol, 12: 260–271

Seibt U, Brand W A, Heimann M, Lloyd J, Severinghaus J P, Wingate L. 2004. Observations of O_2:CO_2 exchange ratios during ecosystem gas exchange. Glob Biogeochem Cycle, 18: GB4024

Severinghaus J P. 1995. Studies of the terrestrial O_2 and carbon cycles in sand dune gases and in Biosphere 2. Doctoral Dissertation. New York: Columbia University

Sirignano C, Neubert R E M, Rödenbeck C, Meijer H A J. 2010. Atmospheric oxygen and carbon dioxide observations from two European coastal stations 2000–2005: Continental influence, trend changes and APO climatology. Atmos Chem Phys, 10: 1599–1615

Sitch S, Friedlingstein P, Gruber N, Jones S D, Murray-Tortarolo G, Ahlström A, Doney S C, Graven H, Heinze C, Huntingford C, Levis S, Levy P E, Lomas M, Poulter B, Viovy N, Zaehle S, Zeng N, Arneth A, Bonan G, Bopp L, Canadell J G, Chevallier F, Ciais P, Ellis R, Gloor M, Peylin P, Piao S L, Le Quéré C, Smith B, Zhu Z, Myneni R. 2015. Recent trends and drivers of regional sources and sinks of carbon dioxide. Biogeosciences, 12: 653–679

Smith W K, Reed S C, Cleveland C C, Ballantyne A P, Anderegg W R L, Wieder W R, Liu Y Y, Running S W. 2016. Large divergence of satellite and Earth system model estimates of global terrestrial CO_2 fertilization. Nat Clim Change, 6: 306–310

Stephens B B, Bakwin P S, Tans P P, Teclaw R M, Baumann D D. 2007. Application of a differential fuel-cell analyzer for measuring atmospheric oxygen variations. J Atmos Ocean Tech, 24: 82–94

Stocker T F, Qin D, Plattner G K L, Alexander V, Allen S K, Bindoff N L, Bréon F M, Church J A, Cubasch U, Emori S, Forster P, Friedlingstein

P, Gillett N, Gregory J M, Hartmann D L, Jansen E, Kirtman B, Knutti R, Krishna Kumar K, Lemke P, Marotzke J, Masson-Delmotte V, Meehl G A, Mokhov I I, Piao S, Ramaswamy V, Randall D, Rhein M, Rojas M, Sabine C, Shindell D, Talley L D, Vaughan D G, Xie S P. 2013. Technical Summary. In: Church J, Clark P, Cazenave A, Gregory J, Jevrejeva S, Levermann A, Merrifield M, Milne G, Nerem R S, Nunn P, Payne A, Pfeffer W T, Stammer D, Alakkat U, eds. Climate Change 2013: The Physical Science Basis. Contribution of Working Group I to the Fifth Assessment Report of the Intergovernmental Panel on Climate Change. Cambridge: Cambridge University Press. 33–115

Sturm P, Leuenberger M, Schmidt M. 2005. Atmospheric O_2, CO_2 and $\delta^{13}C$ observations from the remote sites Jungfraujoch, Switzerland, and Puy de Dôme, France. Geophys Res Lett, 32: L17811

Sun G, Mu M. 2013. Understanding variations and seasonal characteristics of net primary production under two types of climate change scenarios in China using the LPJ model. Clim Change, 120: 755–769

Sun G, Mu M. 2017. Projections of soil carbon using the combination of the CNOP-P method and GCMs from CMIP5 under RCP4.5 in North-South Transect of Eastern China. Plant Soil, 413: 243–260

Sutton M A, Simpson D, Levy P E, Smith R I, Reis S, van Oijen M, de Vries W. 2008. Uncertainties in the relationship between atmospheric nitrogen deposition and forest carbon sequestration. Glob Change Biol, 14: 2057–2063

Tohjima Y, Mukai H, Machida T, Hoshina Y, Nakaoka S I. 2019. Global carbon budgets estimated from atmospheric O_2/N_2 and CO_2 observations in the western Pacific region over a 15-year period. Atmos Chem Phys, 19: 9269–9285

Townsend A R, Braswell B H, Holland E A, Penner J E. 1996. Spatial and temporal patterns in terrestrial carbon storage due to deposition of fossil fuel nitrogen. Ecol Appl, 6: 806–814

Trumbore S E, Czimczik C I. 2008. An uncertain future for soil carbon. Science, 321: 1455–1456

Valentino F L, Leuenberger M, Uglietti C, Sturm P. 2008. Measurements and trend analysis of O_2, CO_2 and $\delta^{13}C$ of CO_2 from the high altitude research station Junfgraujoch, Switzerland—A comparison with the observations from the remote site Puy de Dôme, France. Sci Total Environ, 391: 203–210

van der Laan S, van der Laan-Luijkx I T, Rödenbeck C, Varlagin A, Shironya I, Neubert R E M, Ramonet M, Meijer H A J. 2014. Atmospheric CO_2, $\delta(O_2/N_2)$, APO and oxidative ratios from aircraft flask samples over Fyodorovskoye, Western Russia. Atmos Environ, 97: 174–181

Wang T, Lin X, Peng S, Cong N, Piao S. 2014. Multimodel projections and uncertainties of net ecosystem production in China over the twenty-first century. Chin Sci Bull, 59: 4681–4691

Whittinghill K A, Currie W S, Zak D R, Burton A J, Pregitzer K S. 2012. Anthropogenic N deposition increases soil C storage by decreasing the extent of litter decay: Analysis of field observations with an ecosystem model. Ecosystems, 15: 450–461

Worrall F, Clay G D, Masiello C A, Mynheer G. 2013. Estimating the oxidative ratio of the global terrestrial biosphere carbon. Biogeochemistry, 115: 23–32

Worrall F, Moody C S, Clay G D, Burt T P, Rose R. 2017. The flux of organic matter through a peatland ecosystem: The role of cellulose, lignin, and their control of the ecosystem oxidation state. J Geophys Res-Biogeosci, 122: 1655–1671

Yang X, Wang M. 2001. A simple model in calculating average soil respiration rate and soil carbon density (in Chinese). J Graduate School Chin Acad Sci, 18: 90–96

Yokota T, Yoshida Y, Eguchi N, Ota Y, Tanaka T, Watanabe H, Maksyutov S. 2009. Global concentrations of CO_2 and CH_4 retrieved from GOSAT: First preliminary results. Sci Online Lett Atmos Sola, 5: 160–163

Yu P, Han D, Liu S, Wen X, Huang Y, Jia H. 2018. Soil quality assessment under different land uses in an alpine grassland. Catena, 171: 280–287

Zhou Z, Zhang Z, Zha T, Luo Z, Zheng J, Sun O J. 2013. Predicting soil respiration using carbon stock in roots, litter and soil organic matter in forests of Loess Plateau in China. Soil Biol Biochem, 57: 135–143

Zhu Z, Liu Y, Liu Z, Piao S. 2018. Projection of changes in terrestrial ecosystem net primary productivity under future global warming scenarios based on CMIP5 models (in Chinese). Clim Change Res, 14: 31–39

(Responsible editor: Hongsheng ZHANG)